A Glutamine to Glutamate Mutation at Position 170 (Q170E) in the Rabbit Na^+/Glucose Cotransporter, rSGLT1, Enhances Binding Affinity for Na^+ †

Steven A. Huntley, Daniel Krofchick, and Mel Silverman*

Department of Medicine, University of Toronto, Toronto, Ontario, Canada M5S 1A8

Received November 4, 2005; Revised Manuscript Received February 2, 2006

ABSTRACT: Using cysteine mutagenesis and chemical modification by methanethiosulfonate derivatives, it was demonstrated that the external putative loop, joining transmembrane segments (TM's) IV−V of rabbit Na^+/glucose cotransporter, rSGLT1, forms part of a Na^+ binding and voltage sensing domain. Within this region, exposure to cationic (2-aminoethyl)methanethiosulfonate hydrobromide (MTSEA) inhibited F163C, A166C, and L173C, but anionic sodium (2-sulfonatoethyl)methanethiosulfonate (MTSES) had no effect. Unexpectedly, MTSEA had no effect on Q170C; however, MTSES profoundly altered Q170C charge transfer and turnover, leaving Na^+ and sugar binding affinity unchanged, but mutation of glutamine to anionic glutamate (Q170E) shifted $V_{0.5}$ to positive potentials, suggesting enhanced Na^+ affinity. To clarify the role of glutamine 170 in Na^+ interaction, we embarked on a more detailed investigation of Q170E using the two-microelectrode voltage clamping in *Xenopus* oocytes. Compared to wild-type (wt) rSGLT1, Q170E exhibits (i) a 2-fold decrease in methyl α-D-glucopyranoside affinity (−150 to −90 mV), (ii) a 5-fold increase in Na^+ affinity (−150 to −100 mV) with less voltage dependency, (iii) reduced Na^+ leak, and (iv) two transient current decay constants (τ_{fast}, τ_{slow}) compared to three (τ_{fast}, τ_{medium}, τ_{slow}) for wt, and computer simulation of Q170E pre-steady-state currents with a four-state kinetic model yields parameters similar to wt SGLT1, except for a reduced Na^+ debinding rate constant compared to wt. Taken together, the data strengthen the conclusion that residue 170 lies in the Na^+ pathway and provide the first evidence that it participates in determining Na^+ binding.

The rabbit intestinal Na^+/glucose carrier (rSGLT1)[1] (*1*) serves as an excellent model system to explore mechanisms of ion-coupled transport. Expression of cloned SGLT1 in *Xenopus laevis* oocytes and the use of the two-microelectrode voltage clamp technique have been particularly informative. Steady-state, sugar-induced inward Na^+ currents of the cotransporter yield affinity values for Na^+, and sugar substrate, as well as estimates of substrate coupling stoichiometry (*2*, *3*). Pre-steady-state current traces, acquired in the presence of Na^+ (but not sugar substrate), are inhibited with either excess sugar or the inhibitor phloridzin (pz). Pre-steady-state currents contain information about transition states involved in Na^+ binding/debinding and reorientation of empty carrier across the membrane (*4*, *5*).

Site-directed mutagenesis, as well as comparison of the functional behavior of wt SGLT1 from different species, has identified amino acids of functional importance in Na^+/sugar cotransport (*6*). Also, the C-terminal half of the transporter, specifically the region comprised of transmembrane segments (TM's) X−XIII, has been implicated in sugar permeation (*7*, *8*).

Application of SCAM determined that when any one of three amino acids (F163, A166, and L173) in the putative extracellular loop connecting TM's IV−V is substituted by cysteine, rSGLT1 becomes sensitive to inhibition by the cationic, cysteine-specific sulfhydryl reagent (2-aminoethyl)-methanethiosulfonate hydrobromide (MTSEA) (*9*, *10*). Detailed electrophysiological characterization of F163C, A166C, and L173C led to the proposal that these residues in the putative loop joining TM IV and TM V are critically involved in the Na^+ binding and voltage-sensing properties of SGLT1 (*9*).

Recent characterization of another cysteine mutant in this loop, Q170C (*11*), demonstrated that changes in polarity and charge at position 170 result in quite different functional consequences compared to what is observed following chemical modification at positions 163, 166, and 173, almost certainly reflecting the structural complexity of this region

† This work was supported by CIHR Grant MOP-15267. S.A.H. and D.K. are Ph.D. candidates in the Institute of Medical Sciences at the University of Toronto.

* To whom correspondence should be addressed. Tel: 416-978-7189. Fax: 416-971-2132. E-mail: melvin.silverman@utoronto.ca.

[1] Abbreviations: SGLT1, high-affinity Na^+/glucose cotransporter; rSGLT1, rabbit SGLT1; hSGLT1, human SGLT1; wt SGLT1, wild-type SGLT1; TM, transmembrane segment; αMG, methyl α-D-glucopyranoside; pz, phloridzin; K_M, substrate affinity constant; K_D, phloridzin affinity constant; K_{Na}, Na^+ affinity constant; τ, decay constant; τ_s, slow decay constant; τ_m, medium decay constant; τ_f, fast decay constant; V_h, holding potential; V_t, test potential; $V_{0.5}$, potential at which charge transfer is half-complete; Q_{max}, the maximum charge transferred; Q_{dep}, charge due to depolarizing pulses; Q_{hyp}, charge due to hyperpolarizing pulses; I_{max}, maximal substrate-induced current; n, Hill coefficient; z, steady-state valence; z_{app}, apparent valence of charge movement; k, substrate turnover number; k_{ij}, rate constant of transition from state i to state j, without voltage or ion dependence; K_{ij}, rate constant of transition from state i to state j, with voltage and/or ion dependence; MTS, methanethiosulfonate; MTSES, sodium (2-sulfonatoethyl)methanethiosulfonate; MTSEA, (2-aminoethyl)methanethiosulfonate hydrobromide; MTSET, [2-(trimethylammonium)ethyl]methanethiosulfonate bromide; DTT, dithiothreitol; $Q170C_{MTSES}$, Q170C rSGLT1 reacted with MTSES.

10.1021/bi052267m CCC: $33.50
Published on Web 03/17/2006

of the Na^+ interaction domain (*11*). Of particular interest is the fact that reaction with cationic MTSEA has no effect on Q170C function, but introducing negative charge at position 170 by reacting with anionic sodium (2-sulfonatoethyl)-methanethiosulfonate (MTSES) causes marked reduction in steady-state sugar-induced inward Na^+ currents, without affecting Na^+ or sugar substrate affinity (*9*, *11*). Neither of the cationic agents MTSEA (*9*, *11*) nor membrane impermeant [2-(trimethylammonium)ethyl]methanethiosulfonate bromide (MTSET) (*11*) affects Q170C function, but both protect against MTSES. Reaction of Q170C with MTSES reduces charge transfer and also causes a 60−70% decrease in Q170C turnover, as well as reducing the Na^+ leak (*11*).

In a recent publication, we presented limited electrophysiologic data for a glutamine to glutamate mutation at position 170 (Q170E) in rSGLT1 (*11*). Similar to MTSES-reacted Q170C, introduction of negatively charged glutamate also leads to reduced turnover (*11*). But, instead of an effect on charge transfer, the mutation produces a shift of the Boltzmann $V_{0.5}$ to positive potentials (*11*). On the basis of the evidence in ref *11*, we deduced that position 170 of rSGLT1 is situated within the Na^+ interaction domain in the putative loop between TM's IV and V, at a location such that cotransporter function is substantially influenced by modulation of polarity and introduction of negative charge. Given the importance of this region in cotransporter function, we decided to undertake a more comprehensive evaluation of the steady-state and pre-steady-state behavior of Q170E to compare with wt rSGLT1, Q170C, and Q170C reacted with MTSES ($Q170C_{MTSES}$).

The present study, combined with previous investigations (*11*), confirms that position 170 in rSGLT1 is functionally highly sensitive to introduction of negative charge. Replacement of glutamine by glutamate (Q170E) results in the carrier assuming a preferred outward conformational state compared to wt rSGLT1, leading to complete charge transfer (*11*). Both $Q170C_{MTSES}$ (*11*) and Q170E exhibit substantial reduction in carrier turnover without increasing the duration of empty carrier or Na^+ binding/debinding transitions, implying that the observed reduction in turnover is due to a rate-limiting step occurring in that portion of the transport cycle that involves debinding of Na^+ and glucose at the inside face of the membrane.

But the most interesting functional consequence of the glutamine to glutamate mutation is an increase in Na^+ affinity reflected in (i) a marked shift in the Boltzmann $V_{0.5}$ to positive potentials (*11*), (ii) a K_{Na} voltage dependency which exhibits a much more rapid rate of decrease in K_{Na} at negative voltages than either Q170C or wt rSGLT1 and an ~5× lower K_{Na} value over the range −50 to −150 mV, and (iii) computer simulations in which the major change is a decrease in Na^+ dissociation rate. Taken together, the data offer further confirmation that residue 170 lies in the Na^+ pathway, as previously suggested (*11*), but also advance the first evidence that residue 170 participates in determining Na^+ binding.

MATERIALS AND METHODS

Molecular Biology. The eukaryotic expression vector pMT3 (provided by the Genetics Institute, Boston, MA) was treated with *Pst*I and *Kpn*I to extract the multiple cloning site, generating pMT4. The cDNA of rSGLT1 (provided by M. Hediger) was subcloned into the remaining *Eco*RI site. The Q170E and Q170C mutations were generated via the megaprimer protocol of polymerase chain reaction mutagenesis as described previously and confirmed by sequencing (*9*).

Oocyte Preparation. *X. laevis* were anesthetized in a 0.2% aqueous solution of 3-aminobenzoic acid ethyl ester. Gravid ovarian sacs were removed and then carefully drawn to expose oocytes and allow access to solution. The oocytes were digested for 25−60 min with 2 mg/mL type IV collagenase (Sigma, Oakville, Ontario, Canada). Collagenase was dissolved in modified Barth's saline (MBS) solution supplemented with $MgCl_2$. MBS/Mg^{2+} consists of 0.88 mM NaCl, 1.0 mM KCl, 2.4 mM $NaHCO_3$, 15.0 mM HEPES−NaOH, and 1.0 mM $MgCl_2$, pH 7.4. Postharvest/digestion care involved Leibovitz solution (Sigma) supplemented with 10 mM HEPES, 20 mg of gentamycin, and 0.184 g of L-glutamine, pH 7.4, with 10 mM NaOH.

Oocyte Injection. Q170E rSGLT1 cDNA was delivered to the nucleus, via the animal pole, of the defolliculated oocytes at a concentration of 60 ng/μL. The injected oocytes were stored at 16−18 °C for 4 days or more in Leibovitz solution of the same composition as that used immediately following collagenase treatment. Previously, it was described how a plasmid bearing the mouse plasmid LFI gene for large T-antigen, middle T-antigen, and small T-antigen was co-injected with the Q170C rSGLT1 cDNA to overcome poor expression levels of Q170C (*11*); however, mouse T-antigen plasmid co-injection was not employed with Q170E cDNA, since Q170E typically has expression levels greater than wt rSLGT1.

Two-Microelectrode Voltage Clamp. Voltage clamping and recordings were performed using a GeneClamp 500 amplifier, Digidata 1200B interface, and pClamp 9.0 data acquisition software (Axon Instruments Inc., Union City, CA). Oocytes were impaled with 150 μm borosilicate glass capillary tubes (World Precision Instruments, Sarasota, FL). The capillary tubes were filled with 3 M KCl solution. Oocytes with resting potentials more positive than −30 mV were discarded. Eligible oocytes were constantly superfused with a voltage clamping solution consisting of 100 mM NaCl, 2 mM KCl, 1 mM $MgCl_2$, 1 mM $CaCl_2$, and 10 mM HEPES−Tris base (pH 7.4). This voltage clamping solution was used for all experiments, with the exception of Na^+ titrations and certain pre-steady-state experiments, which examined Na^+ dependence. The rate of superfusion was approximately 3.5 mL/min. The oocyte was held at a holding potential, V_h, of −50 mV and then was subjected to a series of voltage test pulses, V_t. The current responses were recorded with a sampling interval of 200 μs for steady-state experiments, 25 μs for the ramp protocol, and 20 μs for decay analysis. The traces represent pre-steady-state currents generated by the cotransporter, in response to stepping the voltage from the holding potential of −50 mV through a range of test pulses from −150 to +90 mV, in 10 or 20 mV increments. The "off" currents represent the reciprocal current responses when the voltage step is discontinued and returned to the holding potential, −50 mV. For those experiments which required a more accurate measurement of charge transfer, the step function test pulse was replaced by a 5 ms ramp (*11*). The array of ramp pulses mirrors that

of the step protocol. The ramp protocol avoids conditions of measuring apparatus saturation, which typically occurs at early times of the step clamp, when large capacitive currents are produced. Thus, the ramp protocol ensures complete recovery of charge transfer over the entire range of voltages, including the extreme range of depolarizing and hyperpolarizing potentials.

Steady-state parameters were determined with the difference in the steady-state currents obtained before and after exposure to the substrate of interest. Steady-state currents were acquired with test pulses of 300 ms duration. The final 150 ms of a test pulse was selected, and the average current value of this range was acquired. The average current values were plotted versus [substrate] and eq 1 was fit to the curve:

$$I = I_{max}[S]^n/([S]^n + K_{0.5}{}^n) \quad (1)$$

in which S is the substrate of investigation (Na^+, αMG), I_{max} is the maximal current induced at saturating [substrate], n is the Hill coefficient, and $K_{0.5}$ is the Michaelis constant, which is the [S] at which $I = I_{max}/2$, which serves as an approximation of substrate affinity. The calculation of substrate affinity values used the I_{max} values of −150 mV test pulses.

The pre-steady-state current of an expressing oocyte is comprised of both a nonspecific component, due to oocyte membrane capacitance, and an SGLT1-specific component. Isolation of the SGLT1-specific component was accomplished with phloridzin (pz), which is an SGLT1 inhibitor. The current recordings acquired in the presence of saturating pz (200 μM) were subtracted from the recordings acquired in the absence of pz to provide the current due exclusively to rSGLT1. In pre-steady-state experiments we used test pulses of the same values as employed in steady-state protocols; however, the test pulses were of a 150 ms duration. Baseline correction for each trace was accomplished by subtracting the average values for the currents measured in the steady-state region from $t = 145$ ms to $t = 150$ ms. The rSGLT1 pre-steady-state currents for each V_t were integrated over the entire course of the trace to calculate the total charge transferred by the cotransporter. The charge, Q, was plotted as a function of the test pulses, and these $Q(V_t)$ curves were fitted to the two-state Boltzmann relation:

$$Q = -Nez/[1 + \exp(zu(V_t - V_{0.5})) + Q_{dep}] \quad (2)$$

where Q is the total charge transferred, Q_{dep} is the charge due to depolarizing pulses, e is the elementary charge, z is the apparent valence of the movable charge, $V_{0.5}$ is the potential at which half of the total charge transfer is complete, and N is the number of cotransporters expressed at the surface. The term $u = F/RT$; F is Faraday's constant, R is the gas constant, and T is absolute temperature.

The initial mathematical operations were performed with Clampfit (Axon Instruments, Foster City, CA). Results were filtered via a 1 kHz, 5 point Gaussian filter. Additional curve fitting was performed in Origin 6.0 with the Levenberg−Marquardt algorithm.

The pre-steady-state parameters for Q170C rSGLT1, first reported in 2004 (*11*), were calculated by fitting the $Q(V_t)$ curves of individual oocytes with the two-state Boltzmann relation to arrive at parameter values and then calculating average values and standard errors for each parameter. The pre-steady-state parameters for Q170E rSLGT1 were derived using a protocol reported by Krofchick et al. in 2004 (*12*). Instead of fitting each $Q(V_t)$ curve with the two-state Boltzmann relation, the $Q(V_t)$ curves are summed via point-by-point addition of current to provide an aggregate $Q(V_t)$ curve. The aggregate $Q(V_t)$ curve is then fitted with a two-state Boltzmann relation. Such an aggregate data set offers an enhanced signal-to-noise ratio; signal-to-noise ratio increases with the square root of the number of contributing data sets. For an aggregate $Q(V_t)$ curve of 22 oocytes, and using the approximation that there is no substantial difference in expression level, then the signal-to-noise ratio is $SNR_{agg} = (22)^{1/2}SNR_{ind} = (4.7)SNR_{ind}$. The fitting with the two-state Boltzmann relation is performed with ORIGIN 6.0, which provides estimates of the standard errors for the parameters. The error is $\sigma_i = (C_{ii}\chi^2)^{1/2}$, where is C_{ii} is the diagonal element of the variance−covariance matrix. The variance−covariance matrix is defined as $\mathbf{C} = (\mathbf{F}' \times \mathbf{F})^{-1}$, where $\mathbf{F}$ is the Jacobian $\mathbf{F}_{i,j} = \delta f(x_{1i}, x_{2i}, ...; p_1, p_2, ...)/\delta_{p_j}$, in which f is the fitting function for the data set values of the independent variables $x_1 = x_{1i}$, $x_2 = x_{2i}$, ...).

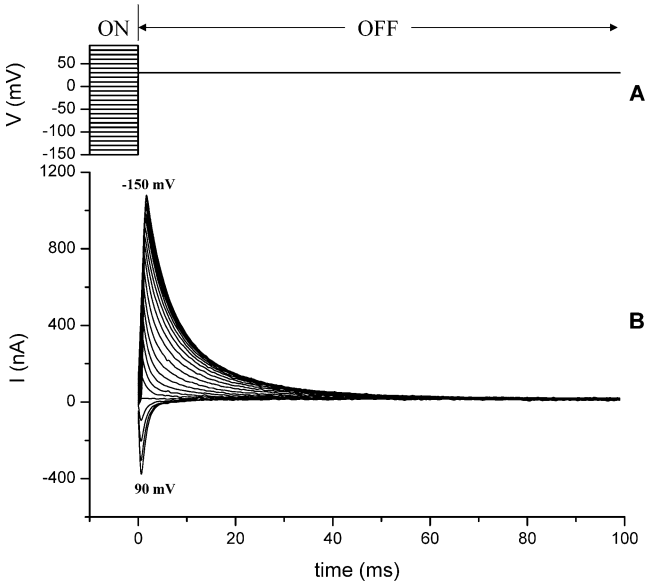

FIGURE 1: Representative transient "off" currents of Q170E rSGLT1 for a 30 mV poststep potential. (A) The waveform used to generate the Q170E transient currents, displayed in (B). The prestep potentials were from −150 to 90 mV, in 10 mV increments, and were applied for a 150 ms duration before the step at $t = 0$ to allow the system to stabilize. At $t = 0$ ms, the desired poststep potential was applied; the representative waveform of (A) has a poststep potential of 30 mV. The poststep potential is applied for a 150 ms duration, from $t = 0$ to $t = 150$ ms. (B) An array of Q170E rSGLT1 poststep transient currents, generated with the waveform described in (A).

Transient Current Measurement. Transient decay parameters of Q170E off currents were derived with the protocol illustrated in Figure 1; this protocol was described in detail by Krofchick and Silverman in 2003 (*13*). The holding potential, V_h, was −50 mV; this potential was maintained between experiments. From −50 mV, the potential was stepped to an array of prestep potentials, or "on" potentials. The prestep potentials were from −150 to 90 mV, in 10 mV increments, and were applied for a 150 ms duration to allow the system to equilibrate. After 150 ms, the desired poststep

potential, or off potential, was applied. A set of poststep potentials was used from −150 to 90 mV, in 20 mV increments; the representative waveform of Figure 1A has a poststep potential of 30 mV. The poststep potential is applied for a 150 ms duration from $t = 0$ ms, in Figure 1, to $t = 150$ ms. Figure 1B shows the first 100 ms of the traces. The resulting array of poststep transient currents, generated with the waveform described, is analyzed for pre-steady-state parameters. The settling time of the voltage clamp was determined by measuring the oocyte membrane potential as a function of time. Voltage steps, ranging from 70 to 240 mV, were investigated. Final potentials were attained from 0.6 ms (70 mV jump) to 1.3 ms (240 mV jump) after the onset of the clamp. Transient currents prior to the settling of the clamp were removed before fitting.

Fitting Decay Currents. Each current trace of a poststep potential was fitted, from $t = 0$ to $t = 150$ ms, to a first-order exponential decay, a second-order exponential decay, and a third-order exponential decay. The order of exponential decay at which the χ^2 value demonstrated no change, or at which the higher order terms became meaningless, was discarded for the previous order of decay. Extremely large or small time constants, amplitude values, or large error values associated with such parameters precluded the validity of a particular order of decay. Several criteria were considered when deciding upon an order of decay. Typically, higher order of decay was accepted if its χ^2 value decreased by ~10% or more, compared to the previous lower order fit. Also, a higher order fit was only deemed valid if the trends observed for such parameters as time constants and amplitude values were consistent over a range of poststep potentials (*13*). Finally, the residuals had to demonstrate a definitive improvement at the highest order fit. The complete details of the technique are provided by Krofchick and Silverman (*13*).

State Model Simulations. State model simulations used transient currents recorded with a 5 ms ramp protocol and a holding potential of −50 mV. At $t = 0$ ms the membrane potential was altered linearly over 5 ms, from the −50 mV holding potential to an array of postramp potentials. At $t =$ 150 ms, the membrane potential was restored to −50 mV via another 5 ms ramp. The employment of a ramp avoids saturation of the measuring apparatus, thereby allowing detection of all current at early times; consequently, transients can be fit from $t = 0$ instead of $t = \sim 1$ ms. Acquired traces were low pass filtered at 1 kHz. Currents following the initial ramp, from $t = 0$ to $t = 150$ ms, were baseline adjusted with the mean current calculated between 145 and 150 ms. Currents following the second ramp, from $t = 150$ to $t =$ 300 ms, were baseline adjusted with the mean current calculated from 295 to 300 ms.

Simulations were performed with the commercially available software package ModelMaker 3 (ModelKinetix, Old Beaconsfield, Buckinghamshire, U.K.). Solutions were based upon the four-state model of Krofchick and Silverman (*13*). There were no assumptions of Na^+ dependence for any of the rate constants. Examination of Na^+-dependent data, involving 10 and 100 mM Na^+, was employed to discern Na^+-dependent transitions. Transient currents at five postramp membrane potentials of −130, −90, −10, 20, and 50 mV were simulated and fit simultaneously from 0 to 50 ms and from 150 to 200 ms. The overall χ^2 was minimized by optimizing 12 parameters: 6 rate constants (k) and 6 valences (z). The likelihood of determining a global minimum was enhanced with an array of initial values for the parameters. Each parameter had two starting values, resulting in $2^{12} =$ 4096 optimizations.

State Model Equations. The four-state model of Krofchick and Silverman (*13*) was simulated with the following set of differential equations:

$$N_1' = -K_{12}N_1 + K_{21}N_2 \tag{3a}$$

$$N_2' = K_{12}N_1 - (K_{23} + K_{21})N_2 + K_{32}N_3 \tag{3b}$$

$$N_3' = K_{23}N_2 - (K_{34} + K_{32})N_3 + K_{43}N_4 \tag{3c}$$

$$N_4' = K_{34}N_3 - K_{43}N_4 \tag{3d}$$

$$N = N_1 + N_2 + N_3 + N_4 \tag{3e}$$

in which N is the total number of expressed transporters and N_i is the number of transporters in state C_i. Eyring rate theory was used to factor voltage dependence, V, of the rate constants (*14*):

$$K_{12} = k_{12}e^{z_{12}uV} \qquad K_{21} = k_{21}e^{-z_{21}uV} \tag{4a}$$

$$K_{23} = k_{23}e^{z_{23}uV} \qquad K_{32} = k_{32}e^{-z_{32}uV} \tag{4b}$$

$$K_{34} = k_{34}e^{z_{34}uV} \qquad K_{43} = k_{43}e^{-z_{43}uV} \tag{4c}$$

in which $u = F/RT$, where F is Faraday's constant, R is the gas constant, and T is temperature in Kelvin. A temperature of 295 K (24 °C) was used, resulting in a u of 0.0394 mV^{-1}. The voltage dependence of each rate constant is characterized by a valence value, z, which is without units. The charge movement associated with a single transition ($C_i \leftrightarrow C_{i+1}$) is the sum of the forward and reverse voltage dependencies:

$$z_i = z_{i,i+1} + z_{i+1,i} \tag{5}$$

Membrane current was calculated with the equation:

$$I = e(z_1(K_{12}N_1 - K_{21}N_2) + z_2(K_{23}N_2 - K_{32}N_3) + z_3(K_{34}N_3 - K_{43}N_4)) \tag{6}$$

in which e is the elementary charge. For simulations, the level of expression, N, was calculated from the Q_{max} of the Boltzmann distribution using the expression:

$$N = Q_{max}/(e(z_1 + z_2 + z_3 + ... + z_i)) \tag{7}$$

Fast−Slow−Fast Model of the SGLT1 Four-State Transient System. Chen et al. in 1996 successfully modeled the four-state system for wt hSGLT1, with the assumption that the second transition is the rate-limiting step (*2*). Krofchick and Silverman demonstrated the validity of this model for wt rSGLT1 (*13*). This assumption can be described by the relation:

$$K_{12} + K_{21} \gg K_{23} + K_{32} \ll K_{34} + K_{43} \tag{8}$$

With this scenario, simple expressions for the time constants are derived (*2*):

$$\tau_1 = 1/(K_{12} + K_{21}) \quad (9a)$$

$$\tau_2 = 1/(K_{23}f + K_{32}g) \quad (9b)$$

$$\tau_3 = 1/(K_{34} + K_{43}) \quad (9c)$$

$$f = K_{12}/(K_{12} + K_{21}) \quad (9d)$$

$$g = K_{43}/(K_{34} + K_{43}) \quad (9e)$$

Statistical Comparisons of Means. The mean values of parameters are presented with standard deviation (mean ± SD). Comparisons of parameters, drawn between wild-type and Q170C rSGLT1, were tested with a two-sample *t*-test for independent samples with equal variances. Comparisons of parameters, before and after exposure to sulfhydryl-specific compounds in the same oocyte, were tested with the paired *t*-test.

RESULTS

Steady-State Behavior of Q170E. As described in the Materials and Methods section, 300 ms test pulses are routinely employed in steady-state experiments, and the steady-state currents are analyzed over the time frame from 150 to 300 ms. These protracted currents allow optimized determination of the average current value during the steady-state region of the traces.

The αMG-induced inward Na^+ currents of Q170E were measured over a range of αMG concentrations; each αMG bathing solution had a saturating [Na^+] of 100 mM. The resulting current (*I*) versus voltage (V_t) curves were transformed to *I* versus [αMG], and the Michaelis−Menten relationship was then fitted to these curves to derive the Michaelis constant, K_M. Q170E K_M values, derived with three oocytes, were plotted as a function of potential, as displayed in Figure 2. The voltage dependence of Q170E αMG affinity displays trends similar to those of Q170C (*11*) and wt rSGLT1 (*9*, *10*). The average Q170E αMG K_M value for the voltage-independent range from −150 to −90 mV is 0.29 ± 0.01 mM ($n = 3$). For the same voltage range, −150 to −90 mV, the average αMG K_M for Q170C is 0.10 ± 0.01 mM ($n = 4$) (*11*), and the average value for wt rSGLT1 αMG K_M is 0.15 ± 0.024 mM ($n = 3$) (*9*). The Q170E K_M value is significantly different from both of the K_M values of Q170C and wt rSGLT1 ($p < 0.0005$), representing an ~2-fold decrease in sugar affinity.

Previously, it was reported that the $Q(V_t)$ curve of Q170E and its fitted Boltzmann relation are significantly shifted to positive potentials compared to those of Q170C ($\Delta V_{0.5}$ = ~40 mV) and wt rSGLT1 ($\Delta V_{0.5}$ = ~25 mV) (*11*), a finding consistent with enhanced Na^+ binding. To further explore the Q170E interaction with Na^+, we carried out a series of Na^+ titration experiments.

The current versus [Na^+] curves (obtained at saturating 10 mM αMG), for a representative expressing oocyte, are displayed in Figure 3A. The Hill equation was fitted to these curves, for three oocytes, which permitted derivation of the Hill coefficients and Na^+ affinity values (K_{Na}). The Hill coefficients displayed voltage dependence from −150 to −10 mV (data not shown). The values ranged from a maximum of 2.3 ± 0.35, for −120 mV, to a minimum of 1.4 ± 0.01, for −40 mV, suggesting that Q170E has a stoichiometry of at least two Na^+/transport cycle, the same as wt rSGLT1.

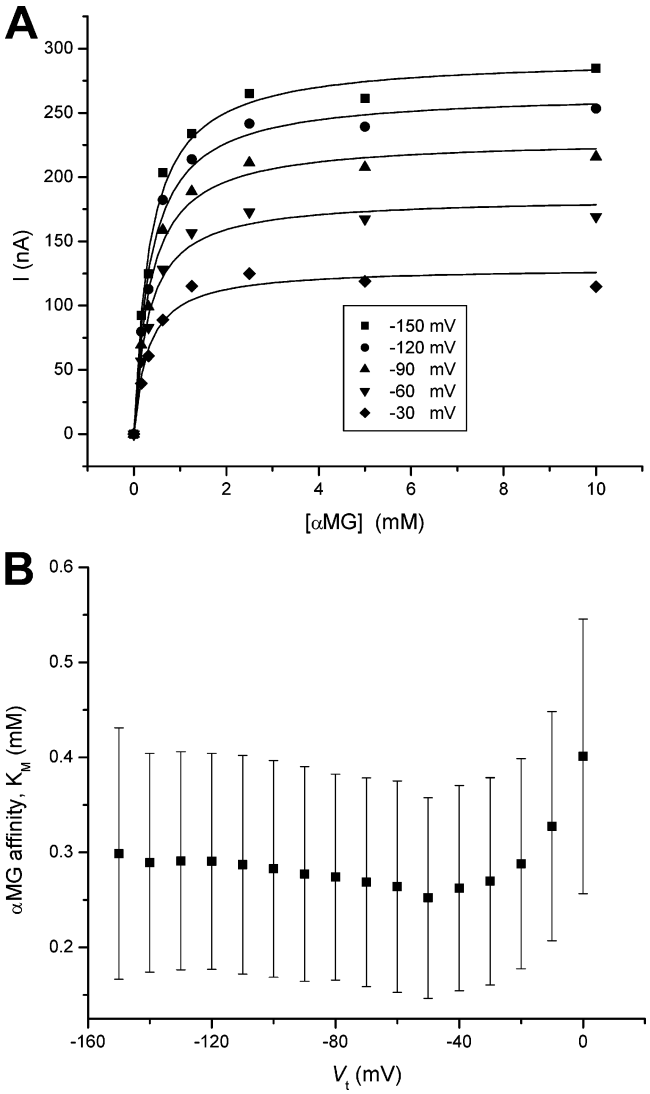

FIGURE 2: Steady-state kinetics of Q170E: Determination of K_M, the αMG affinity value of Q170E rSGLT1. Expressing oocytes were voltage-clamped, and αMG titrations were performed using solutions with saturating 100 mM Na^+ and αMG concentrations ranging from 0 to 10 mM. All titration solutions were of pH 7.4. (A) Typical results from a single oocyte showing αMG dependence of Q170E steady-state currents for V_t values of −150, −120, −90, −60, and −30 mV. The data from the αMG titration were transformed to examine the αMG dependence of the steady-state currents for V_t values, ranging from −150 to −10 mV, inclusive. Each curve was fitted with the Michaelis−Menten equation, $I = I_{max}[S]/([S] + K_{0.5})$, where I_{max} = current at −150 mV, to yield values for affinity, K_M ($K_{0.5}$). (B) Voltage dependence of the αMG affinity of Q170E. The V_t's from −150 to −10 mV, inclusive, are plotted versus [αMG].

The Q170E K_{Na} values were plotted as a function of potential, as displayed in Figure 3B. The Na^+ affinity of Q170E is greater than the affinities of either Q170C or wt rSGLT1. The Q170E K_{Na} values display voltage dependency such that Na^+ affinity decreases (i.e., K_{Na} values increase) with increasing positive potentials. Although Q170C (*11*) and wt rSGLT1 (*3*, *9*, *10*) also exhibit decreasing Na^+ affinities with increasing positive potentials, the Q170E K_{Na} voltage dependence is significantly different from that observed for Q170C and wt rSGLT1. Figure 3B presents a comparison of the voltage dependency of the K_{Na} values of

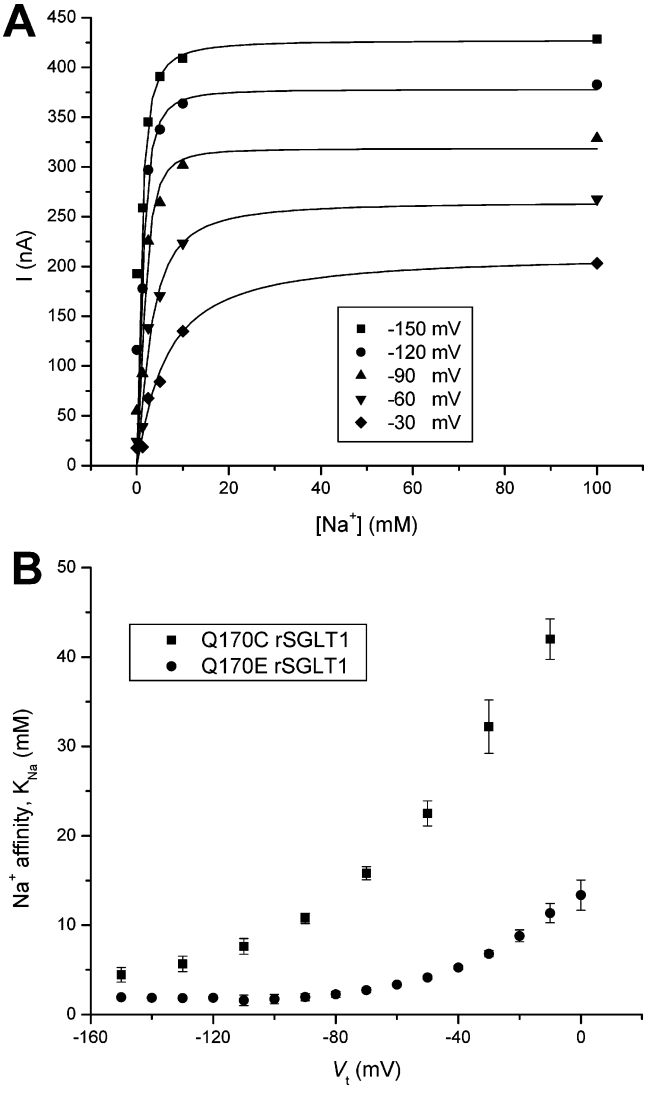

FIGURE 3: Steady-state kinetics of Q170E: Determination of K_{Na}, the Na^+ affinity of Q170E rSLGT1. Expressing oocytes were voltage-clamped, and Na^+ titrations were performed using solutions with saturating αMG (10 mM) and Na^+ concentrations ranging from 0 to 100 mM. The voltage-clamping solutions were supplemented with appropriate concentrations of choline to provide a cation concentration of 100 mM. All titration solutions were of pH 7.4. (A) Typical results from a single oocyte showing Na^+ dependence of Q170E steady-state currents for V_t values of −150, −120, −90, −60, and −30 mV. The data from the Na^+ titration were transformed to examine Na^+ dependence of the steady-state currents for V_t values, ranging from −150 to −10 mV, inclusive. Each curve was fitted with the Hill equation, $I = I_{max}[Na^+]^n/([Na^+]^n + K_{0.5}^n)$, where I_{max} = current at −150 mV, to yield values for affinity, K_{Na}, and the Hill coefficient, n. (B) Voltage dependence of the Na^+ affinity of Q170E (●). The voltage dependence of Na^+ affinity of Q170C (■) is also provided for comparison. The V_t's from −150 to −10 mV, inclusive, are plotted versus $[Na^+]$. Exponential analysis yielded τ values of 35 for Q170E and 65 for Q170C.

Q170C and Q170E. The marked shift of the Q170E K_{Na} curve to positive potentials relative to that for Q170C, the rapid exponential decline, and the near voltage independence over hyperpolarization potentials provide convincing evidence that the presence of the negatively charged glutamate residue at position 170 has substantially increased apparent Na^+ affinity.

The effect of the Q170E mutation on Na^+ leak was considered. The 170 residue is near the Na^+ interaction region (*9*); therefore, it is informative to observe the effects of charge and polarity at 170 on the Na^+ leak. The negative ethylsulfonate of $Q170C_{MTSES}$ reduces Na^+ leak by more than 50% compared to Q170C (*11*). To permit a comparison of Q170E leak current to wt leak, the Na^+ leak was normalized by fitting the corresponding $Q(V_t)$ curves with a two-state Boltzmann relation to derive the Q_{max}. The Q_{max} served as a gauge of expression. As with $Q170C_{MTSES}$, the Q170E mutation reduces the Na^+ leak by greater than 50% (data not shown).

Thus, in marked contrast to Q170C or $Q170C_{MTSES}$, which show little change in substrate affinity either for sugar or Na^+, Q170E demonstrates ~2-fold reduction in sugar affinity and a significant increase in Na^+ affinity (~5-fold from −50 to −150 mV).

Pre-Steady-State Behavior of Q170E. Q170E Charge-Transfer Characteristics. Pre-steady-state parameters for Q170E were previously published, which were derived from the data of four oocytes (*11*). To provide a more robust data set to be used for comparison with computer modeling simulations, Q versus V_t data from 22 oocytes were combined with a point-by-point addition of charge to create an aggregate $Q(V_t)$ curve (Figure 4). As described by Krofchick et al. (*12*), an aggregate $Q(V_t)$ curve offers the benefit of enhanced signal-to-noise ratio; signal-to-noise ratio increases by the square root of the number of trials comprising the data set. The aggregate $Q(V_t)$ curve was fitted with a two-state Boltzmann relation to obtain the various pre-steady-state parameters [note: the two-state Boltzmann relation fit derived with Origin 6.0 is not shown; instead, the $Q(V_t)$ fits displayed in Figure 4 are the simulated two-state Boltzmann relation fits, which will be addressed in the section on model simulations]. The Q170E $Q(V_t)$ curve and fitted Boltzmann relation reveal a shift of $V_{0.5}$ to positive potentials with a mean value of 21.7 ± 1.4 mV (n = 22); z = 1.18 ± 0.05. Q170E Q_{dep}/Q_{max} is 91 ± 3%, which is significantly different from the wt value of 86 ± 2% ($p < 0.005$) and demonstrates that the Q170E mutation elicits a cotransporter conformational distribution with a greater number of cotransporters at the outside-facing conformation, compared to wt, at V_h = −50 mV. Q_{hyp} saturation and an unchanged z value suggest that the Q170E mutation has very little effect on charge transfer, unlike $Q170C_{MTSES}$.

The Na^+ dependence of the relative contributions of Q_{hyp} and Q_{dep} to Q_{max} was next investigated. Figure 5 presents the Q170E $Q(V_t)$ curves for 100 and 10 mM Na^+, obtained from three oocytes. Lowering $[Na^+]$ to 10 mM results in loss of charge in the Q_{dep} region. This loss is expected since reducing external Na^+ causes proportionate increases in the number of inward-facing cotransporters, at the −50 mV holding potential. With fewer cotransporters in an outside-facing conformation at V_h −50 mV, there will be less charge generated by cotransporters moving to an inside-facing conformation with depolarizing pulses. This loss in Q_{dep} with decreasing external $[Na^+]$ was previously observed with Q170C and wt rSGLT1 (*11*). For conservation of charge we would expect that loss in Q_{dep} would be regained in Q_{hyp}, since cotransporters in an inside-facing conformation at V_h −50 mV would move to an outside-facing conformation with hyperpolarizing pulses. Inspection of Figure 5 shows that there is indeed a gain in the hyperpolarizing region when the external $[Na^+]$ is reduced to 10 mM. Therefore, when $[Na^+]$ is reduced to 10 mM, there is a preservation of charge

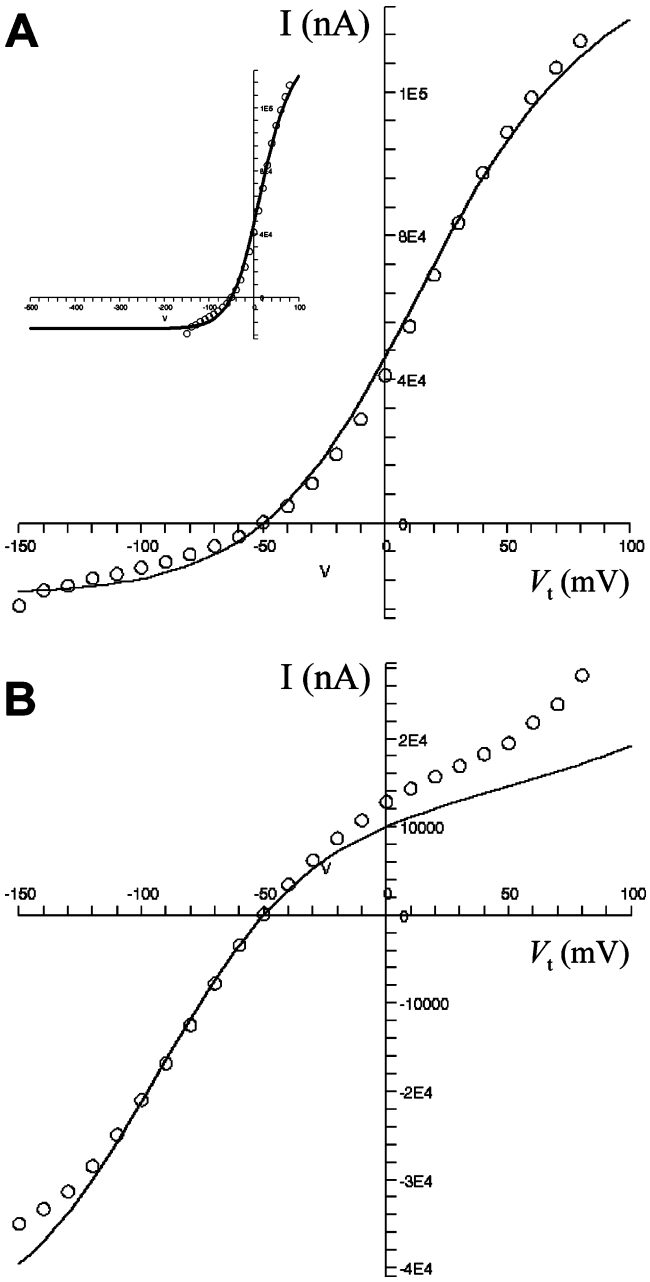

FIGURE 4: Experimental Q versus V_t curves and *simulated* Boltzmann relations of Q170E rSLGT1 for 100 and 10 mM Na^+. The experimental $Q(V_t)$ curves of Q170E are represented with the circular data points. $Q(V_t)$ curves were derived with a ramp protocol as described in the Materials and Methods section. The ramp protocol used V_t's from −150 to 90 mV, in 10 mV increments. The currents were baseline-adjusted from $t = 145$ ms to $t = 150$ ms. Integration was then performed from 0 to 150 ms. An enhanced signal-to-noise ratio was achieved via the summation of individual $Q(V_t)$ curves to yield an aggregate $Q(V_t)$ curve. The simulated Boltzmann relations were achieved with the substitution of the parameter values displayed in Table 1 into eqs 9a−e and then solving for the eigenvalues of the system using Maple 9.00. (A) The aggregate $Q(V_t)$ curve for 100 mM Na^+, $n = 22$ oocytes, and the simulated Boltzmann relation. (B) The aggregate $Q(V_t)$ curve for 10 mM Na^+, $n = 6$ oocytes, and the simulated Boltzmann relation.

transfer for Q170E rSLGT1. The inset of Figure 5 displays the same Q170E $Q(V_t)$ curves for 100 and 10 mM Na^+, after being zeroed and normalized to the 100 mM Na^+ curve, and demonstrates conservation of charge at reduced [Na^+]. The derived Q_{max} from the fitted Boltzmann relation of the 10

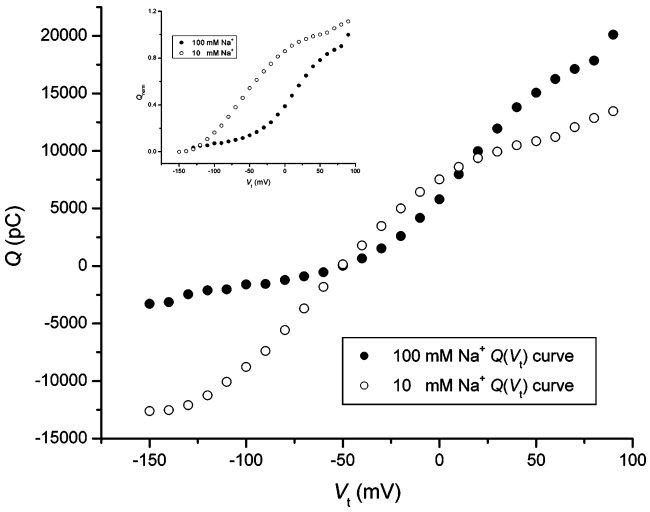

FIGURE 5: Comparison of the effects of 10 and 100 mM Na^+ upon the $Q(V_t)$ curves of Q170E rSLGT1. The $Q(V_t)$ curves were acquired in 10 and 100 mM Na^+ with the same oocyte. A ramp protocol was employed, as described in the Materials and Methods section. The $Q(V_t)$ curves were summed for each [Na^+]. Three expressing oocytes were used. (Inset) The $Q(V_t)$ curves for each [Na^+] were zeroed and normalized to the 100 mM Na^+ $Q(V_t)$ for a direct comparison of the Q_{max} values.

mM Na^+ $Q(V_t)$ curve is 103% compared to the derived Q_{max} of the 100 mM Na^+ curve. For comparison, charge recovery for wt under identical conditions is 81% and for Q170C is 22% (*11*).

Time Constants of Pre-Steady-State Currents for Q170E. As described in the Materials and Methods section and illustrated in Figure 1, an off current protocol (*13*) was employed to determine the time constants of pre-steady-state currents. This protocol takes advantage of the fact that rates of decay are exclusively a function of the poststep potential. Therefore, each poststep potential generates a family of curves with the same time constants, allowing for accurate analysis as described in the Materials and Methods section. Figure 6 shows a representative decay current for Q170E rSGLT1; specifically, the decay current is that of a prestep potential of −130 mV to a poststep potential of 30 mV, with a 100 mM Na^+ perfusion solution. The transient current was fitted with first-, second-, and third-order decay exponentials, which are presented in Figure 6. Inspection of Figure 6A reveals that a first-order decay exponential, represented with a solid line, is inadequate to properly fit the transient. Figure 6B displays the first-, second-, and third-order exponential fits on a different time scale, from 0 to 10 ms. For clarity, the data have been removed from Figure 6B, leaving only the exponential fits. Figure 6B demonstrates that a second-order decay exponential fits the data very well and that a third-order decay exponential offers no further benefit; indeed, the second- and third-order fits overlap. The sufficiency of the second-order fit for the −130 to 30 mV transient is further confirmed by calculation of the residuals (difference between data and the best fit), for the first-, second-, and third-order exponential fits, displayed in Figure 7. Figure 7A is the residual calculation for the first-order exponential fit; there are nonrandom regions at early times, up to ~50 ms. Therefore, first-order exponential decay does not accurately describe the current trace of Figure 6. The second-order residual calculation, presented in Figure 7B, demonstrates random oscillations for the full time course,

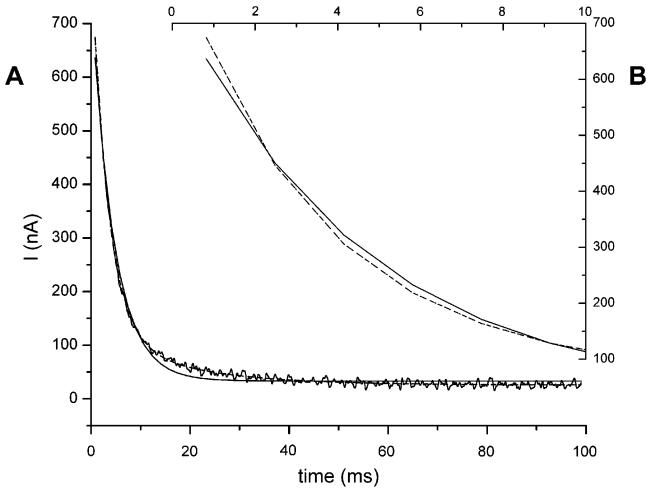

FIGURE 6: Comparison of various orders of exponential decay fits to a transient decay. The transient decay is that of a prestep potential of −130 mV to a poststep potential of 30 mV. (A) First- (solid line), second- (dashed line), and third-order (dotted line) fits are presented with the decay trace. The first-order decay exponential fit is clearly inadequate to describe the transient. (B) The exponential fits of (A) are presented on a different scale, from 0 to 10 ms, to give a better view of the second- and third-order fits. The actual data points have been removed to provide clarity.

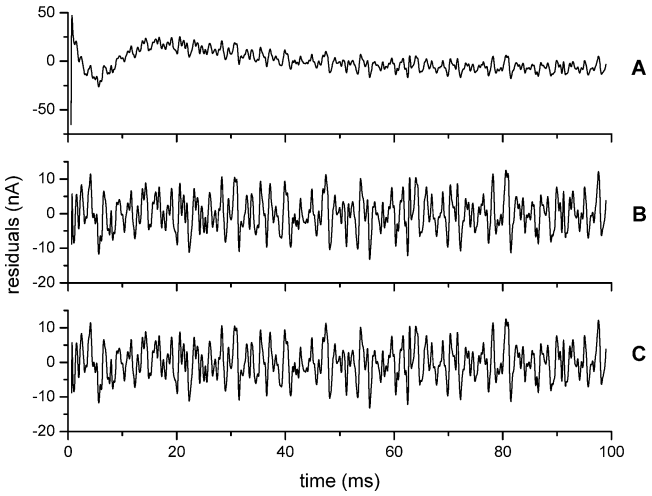

FIGURE 7: The fit residuals. First- (A), second- (B), and third-order (C) fit residuals for the −130 mV prestep, 30 mV poststep potential transient presented in Figure 6. The residuals are calculated as data minus fit. A good fit results in noise only, so the residual oscillates randomly about the zero axis. The residual of the first-order exponential decay fit has regions, which are nonrandom. However, the second-order fit yields a residual comprised of random noise. A third-order fit is superfluous.

which indicates adequate fitting. Indeed, the third-order residual calculation of Figure 7C is identical to the second order.

In previous analyses of wt SGLT1, the transients were defined by three time constants, τ (τ_{slow}, τ_{med}, and τ_{fast}), representing, respectively, slow, medium, and fast transitions. The glutamine to glutamate mutation (Q170E) has altered the transition states of the transporter so that, under the same experimental conditions and apparatus as used to evaluate wt SGLT1, the τ_{fast} is detectable in Q170E but too fast to measure with any confidence. Instead, at all depolarizing V_t traces, two time constants dominate. These conform to the slow and medium time constants previously defined for wt. Therefore, for consistency and to facilitate comparison of

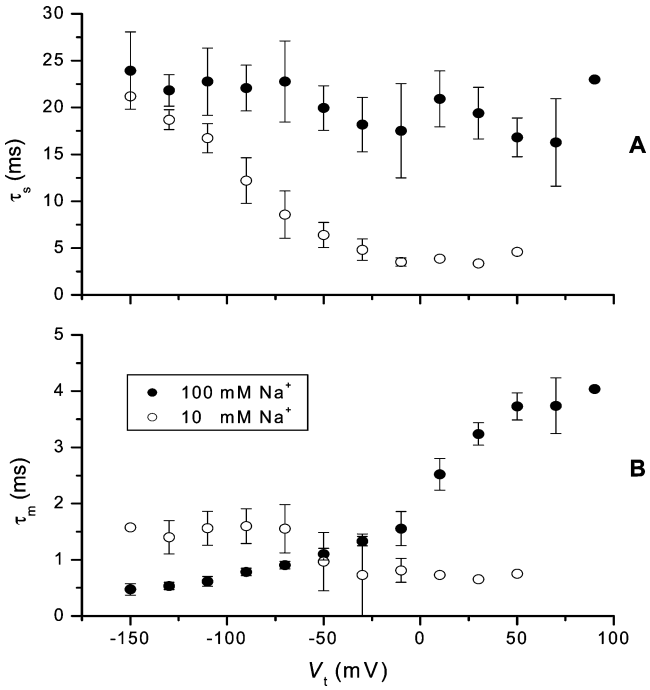

FIGURE 8: Voltage and Na^+ dependencies of the decay constants derived for Q170E rSGLT1 transient currents: (A) τ_s, slow decay constant; (B) τ_m, medium decay constant. The value of n is the number of different oocytes in which measurements were successfully carried out at a given off potential, V_t. Error bars represent standard deviation for data points of $n \geq 3$, and for $n = 2$, points are the average value and error bars represent the range of the difference. (●) 100 mM Na^+ data set: V_t −110 mV, $n = 5$; V_t's −150, −130, −90, −70, and −50 mV, $n = 4$; V_t's −30, −10, 10, 30, 50, and 70 mV, $n = 3$; V_t 90 mV, $n = 1$. (○) 10 mM Na^+ data set: V_t's −150, 10, 30, and 50 mV, $n = 1$; V_t's −130, −110, −90, −70, and −10 mV, $n = 2$; V_t's −50 and −30 mV, $n = 3$.

Q170E with wt SGLT1 with regard to pre-steady-state function, we have retained the nomenclature used for wt (*13*) and denote the second-order decay exponentials obtained from Q170E transient analyses as τ_{slow}, the slow decay constant, and τ_{med}, the medium decay constant.

The voltage dependencies of the decay constants of Q170E are presented in Figure 8. Noteworthy is the fact that τ_{slow} is decreased by about 50%, i.e., ∼2× faster compared to τ_{slow} for Q170C (*11*) or wt (*13*), and is essentially voltage independent at negative potentials at 100 mM Na^+. Interestingly, at 10 mM Na^+, τ_{slow} becomes voltage dependent, increasing at hyperpolarizing potentials. Qualitatively, the relationship of τ_{slow}, under high and low Na^+, is similar to that of wt (*13*), except that τ_{slow} is reduced and there is less voltage dependency at the higher Na^+ concentration. τ_{med} is relatively unchanged in magnitude and also exhibits voltage dependency as previously observed for wt (*13*).

The Q170E rSGLT1 experimentally resolved time constants are interesting, when considered in the context of the previously published turnover values for Q170E and wt rSGLT1. The turnover value of Q170E was determined to be 11.6 ± 2.5 s^{-1} (*11*) compared to a wt turnover number of 22.8 ± 0.5 s^{-1} (*10*). Consequently, the measured decrease in Q170E decay constants, in the present study, suggests that the transition states associated with Na^+ binding/debinding or reorientation of empty carrier are not rate limiting.

Computer Model Simulations of Q170E Pre-Steady-State Currents. Computer model simulations were employed to gain further insight into the functional differences between Q170E rSGLT1 and wt rSGLT1. Although transient current analysis of Q170E resolved two, instead of three decay components, we chose a four-state model (depicted in Figure 10), under the assumption that a third transition was present but too fast for detection; also a four-state model was thoroughly examined by Chen et al. for wt hSGLT1 (*2*) and by Krofchick and Silverman for wt rSLGT1 (*13*) and therefore provided a valuable initial reference.

Transient currents were recorded for postramp potentials of −130, −90, −10, 20, and 50 mV for [Na^+]'s of 10 and 100 mM. These experimental currents were fitted with simulated model currents. Na^+ dependence was not assigned to any of the transitions; Na^+-dependent transitions become evident when a given parameter has two different values for different [Na^+]'s. A rate constant governing an ion binding event is described with the equation:

$$k = k'[\mathrm{A}]^n$$

in which A is the ion species, k' is the rate constant in the absence of ion, and n is the order of the binding event. Therefore, if [Na^+] is reduced from 100 to 10 mM, a rate constant describing a first-order binding event will decrease 10-fold, whereas a rate constant describing a second-order binding event will decrease 100-fold.

Figure 9 compares the experimental transient current recordings obtained for postramp potentials of −130, −90, −10, 20, and 50 mV for 10 and 100 mM Na^+, with currents simulated by the four-state model. Table 1 presents a summary of representative model parameters for Q170E rSLGT1 at 10 and 100 mM Na^+. The results of the multiparametric fitting are typical of the fits achieved with four different oocytes for 100 mM Na^+ and three different oocytes for 10 mM Na^+. We were able to fit the 100 and 10 mM Na^+ data with the same set of parameters, except for k_{12}, k_{21}, and k_{23}, which required assignment of different values for 100 and 10 mM Na^+ conditions.

The Q170E parameter values in Table 1 were entered into eqs 9a−e, and the eigenvalues of the system were solved using the software Maple 9.00 (Waterloo Maple Inc., Waterloo, Ontario, Canada) in order to reconstruct Q170E experimental pre-steady-state results [i.e., $Q(V_t)$ curves and τ versus V curves]. The theoretical τ versus V plots revealed that the magnitudes and voltage dependencies of both the τ_s and τ_m are well simulated with the solution sets of Table 1 for both 100 and 10 mM Na^+ (data not shown). The amplitudes of the theoretical decay constants also simulate the experimental amplitudes to a reasonable degree (data not shown). The least successful fit was the simulated τ_m profile for 10 mM Na^+, which was comparable in magnitude (∼0.7−1.5 ms) to experimental data, but with a different voltage dependency. This disparity in the voltage dependence is likely a consequence of the speed of the transition; i.e., the transition is slow enough to detect but is too fast to resolve with great accuracy.

As displayed in Figure 4, the simulated Boltzmann relations conform well to the experimental data for both 100 and 10 mM Na^+. The $Q(V_t)$ curve and simulated Boltzmann relation for 100 mM Na^+ are particularly in good agreement.

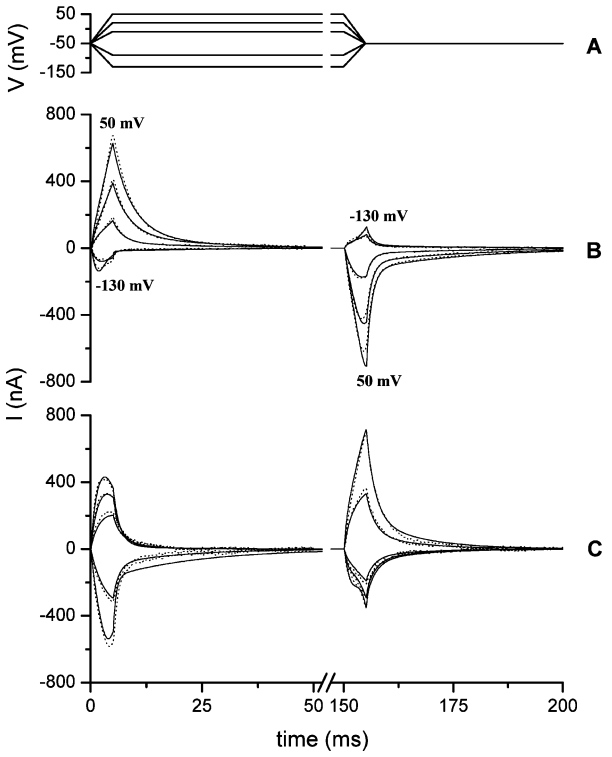

FIGURE 9: Modeling ramp protocol with the experimental transient currents and simulated currents. (A) The waveform used to generate the transient currents in (B) and (C). At $t = 0$ ms, a 5 ms linear ramp was applied from the V_h of −50 mV to postramp potentials of −130, −90, −10, 20, and 50 mV. At $t = 150$ ms, another 5 ms linear ramp was used to restore potential to −50 mV. Postramp potentials more hyperpolarizing than −50 mV generated negative transient currents; postramp potentials more depolarizing than −50 mV generated positive transient currents. (B) The experimental and simulated transient currents of Q170E rSGLT1 for 100 mM Na^+. (C) The experimental and simulated transient currents of Q170E rSGLT1 for 10 mM Na^+.

Table 1: Four-State Model Solutions for Q170E rSGLT1

	[Na^+]	k_{12}	k_{21}	k_{23}	k_{32}	k_{34}	k_{43}
Q170E rSGLT1	100	85	240	45	45	200	1900
	10	360	600	100	45	200	1900
	[Na^+]	z_{12}	z_{21}	z_{23}	z_{32}	z_{34}	z_{43}
Q170E rSGLT1	100	0.24	0.56	0	0	0.0	0.42
	10	0.24	0.56	0	0	0.0	0.42
	[Na^+]	k_{12}/k_{21}		k_{23}/k_{32}		k_{34}/k_{43}	
rSGLT1[a]	100	0.367		4.167		0.868	
	10	20.9					
Q170E rSGLT1	100	0.354		1.00		0.105	
	10	0.600		2.22			

[a] Parameter values are from Krofchick and Silverman (*13*).

The two curves share similar $V_{0.5}$ and z values and exhibit no saturation at experimental depolarizing V_t's. The curves deviate in the extreme hyperpolarizing region. The experimental data display an inflection point at ∼−110 mV, but the simulated Boltzmann relation does not. This may indicate an experimental anomaly or that the system is not yet saturating. However, because this particular mutant has a tendency toward an outside-facing conformational state, as evidenced by the Q_{dep}/Q_{total} data, saturation is expected within the experimental range. To further examine the question of saturation, the simulated Boltzmann relation was extrapolated

in Maple 9.00, well past −150 mV, to −500 mV (Figure 4A inset). The simulated Boltzmann relation predicts saturation beyond −150 mV. It is unlikely, then, that lack of saturation is responsible for the inflection point.

The Q170E $Q(V_t)$ data and the simulated Boltzmann relation for 10 mM Na^+ exhibit good overall concurrence. The hyperpolarizing region, in particular, demonstrates good agreement, indicating lack of saturation. The depolarizing region also is reasonable, with both the $Q(V_t)$ curve and the simulated Boltzmann curve indicating lack of saturation in the region. However, the simulated Boltzmann curve shows less charge in the depolarizing region. This suggests that the model may be underestimating one or more *z* values of the empty carrier transitions.

Comparison of the multiparametric fittings of the presteady-state currents for Q170E and wt rSGLT1, displayed in Table 1, indicates that the principal effect of the glutamine to glutamate mutation is reflected in the k_{12}/k_{21} ratio. As expected and exemplified for wt, when the Na^+ concentration is reduced by a factor of 10, k_{21}, the binding rate for Na^+, should decrease by roughly the same amount and the ratio k_{12}/k_{21} will increase 10 times, which is observed in Table 1. But for Q170E, when the sodium concentration is reduced by a factor of 10, the observed change in the k_{12}/k_{21} ratio is less than two times, suggesting that the mutation has resulted in an increase in k_{21}, the on rate, or binding rate, for Na^+.

DISCUSSION

The objective in the present study was to expand investigation of Q170E function to help to clarify the role of glutamine 170 within the Na^+ interaction domain (*9*, *10*). In this context, it is useful to contrast the properties of Q170E with Q170C in the absence and presence of chemical modification by MTS reagents. Before undertaking a detailed comparison, however, it is important to recall that neither the mildly membrane-permeant MTSEA nor membrane-impermeant compounds MTSES and MTSET exert any influence on wt rSGLT1 function (*9*, *10*).

In previous studies (*9*, *11*), it was demonstrated that exposure to anionic MTSES profoundly alters Q170C rSGLT1, while cationic MTSEA and MTSET are each without effect, yet block the action of MTSES. There are two possible explanations for this protective effect: (i) MTSET and MTSEA react with the exogenous cysteine at 170, directly blocking MTSES accessibility/reactivity, or (ii) MTSES accessibility/reactivity to exogenous cysteine 170 is reduced due to an indirect conformational change brought about in response to MTSET or MTSEA reacting with one or more of the 15 native cysteines in rSGLT1. Since MTSET is membrane impermeant, it would be expected to interact only with native extracellular cysteines (i.e., C255, C345, C351, C355, C361), in addition to the extracellular cysteine introduced at position 170. But, as reported by Huntley et al., MTSET has no effect on Q170C charge transfer (i.e., the Boltzmann relation is unchanged) (*11*). Therefore, MTSET protection against MTSES could only take place by MTSET interfering with MTSES accessibility/reactivity with cysteine 170 in Q170C. We conclude that it is the presence of a negative ethylsulfonate group at the 170 position, arising out of reaction with MTSES, which causes altered function of the chemically modified Q170C (*11*).

It is interesting to compare consequences to rSGLT1 function when negative charge is introduced at position 170 via different means: MTSES reacted Q170C ($Q170C_{MTSES}$), with a lengthy ethylsulfonate group at cysteine 170 (*11*), versus the glutamine to glutamic acid mutation (Q170E), characterized in the present study.

There are similarities in Q170E and $Q170C_{MTSES}$ function:

(i) Both $Q170C_{MTSES}$ (*11*) and Q170E exhibit reduced Na^+ leak.

(ii) Both $Q170C_{MTSES}$ and Q170E exhibit reduced turnover number, although the turnover of $Q170C_{MTSES}$ is reduced to a greater degree (*11*).

(iii) Both $Q170C_{MTSES}$ and Q170E exhibit transient current decay constants which are either unchanged ($Q170C_{MTSES}$) (*11*) or are faster (Q170E) compared to those of wt rSGLT1, implying that reduced turnover number is due to an effect at a rate-limiting step preceding formation of the inside-facing empty carrier, C_4, and is not due to effects on the transitions of empty carrier reorientation or Na^+ binding/debinding.

Several informative differences in Q170E and $Q170C_{MTSES}$ function also emerged:

(i) There are differences in the substrate affinity values for Q170E and $Q170C_{MTSES}$. Following exposure to MTSES, the inward Na^+ currents of Q170C are reduced by approximately half. Such low levels of current do not afford sufficient resolution for sugar titration experiments; therefore, αMG affinity values are not available for $Q170C_{MTSES}$. However, titration experiments were performed with pz, which is the competitive inhibitor of SGLT1. Values of pz affinity serve as a means to gauge effects on the sugar interaction domain. The pz titrations showed that $Q170C_{MTSES}$ and wt rSGLT1 have equivalent pz affinity values, K_D (*11*); $Q170C_{MTSES}$ also has a comparable Na^+ affinity compared to wt (*11*). However, sugar affinity is reduced for Q170E by a factor of ∼2, while Na^+ affinity is increased by a factor of ∼5 with a marked shift in the K_{Na} versus voltage curve toward positive potentials.

(ii) The voltage-dependent charge-transfer characteristics, as gauged by the $Q(V_t)$ curves, are different for $Q170C_{MTSES}$ and Q170E. For $Q170C_{MTSES}$, there is a substantial reduction in charge transfer; for Q170E, charge transfer is complete, but the Boltzmann $V_{0.5}$ is shifted to positive potentials, consistent with increased affinity for Na^+ (*11*).

(iii) Finally, although transient currents of Q170C are reduced significantly following MTSES exposure, thereby making decay constant resolution difficult, those analyses which were performed revealed three transient time constants for $Q170C_{MTSES}$, comparable to those of wt SGLT1 (*11*), whereas Q170E has two time constants, the fast component, τ_{fast}, appears to be missing and τ_{slow} is actually faster and voltage independent at 100 mM Na^+ (Figure 8).

The functional alterations that take place in response to mutation and chemical modification at position 170 also need to be interpreted in the context of functional changes that take place as a result of mutagenesis and chemical modification at neighboring residues in the external loop joining TM's IV−V. In particular, the contrast between the increased apparent Na^+ affinity phenotype conferred by the glutamine to glutamic acid mutation and the reduced Na^+ interaction exhibited by MTSEA-reacted F163C, A166C, and L173C (*9*) requires explanation. Because the sulfhydryl group of

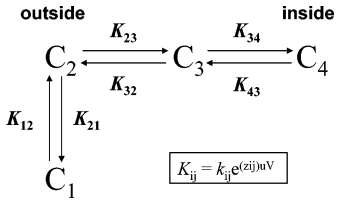

FIGURE 10: Four-state model of SGLT1 in the absence of sugar substrate. Chen et al. in 1996 (*2*) proposed this pre-steady-state model for hSGLT1, which incorporates an experimentally determined intermediate empty carrier state between inside facing and outside facing. The model has two outside-facing conformational states, C_1 and C_2; an inside-facing conformation, C_4; and a conformation intermediate to outside facing and inside facing, C_3. C_1 is the outside-facing/Na^+-bound state; C_2, C_3, and C_4 are all empty carrier conformations. Therefore, there are three transitions: a Na^+ binding/debinding, outside-facing transition, $C_1 \leftrightarrows C_2$; and two empty carrier transitions across the membrane, $C_2 \leftrightarrows C_3$ (outside-facing empty carrier to intermediate state) and $C_3 \leftrightarrows C_4$ (intermediate to inside-facing state). At the holding potential, $V_h = -50$ mV, the majority of transporters are outside facing with Na^+ bound, i.e., in C_1. With depolarizing pulses (more positive than -50 mV) Na^+ debinds, and the cotransporters move toward the inside-facing conformation, C_4. Greater degrees of depolarization effect greater migration of carriers toward the inside-facing conformation. Pulses more hyperpolarizing (more negative) than $V_h = -50$ mV cause those cotransporters not in C_1 to move toward C_1. The rate constants for the transitions are displayed.

Q170C is accessible to impermeant MTSET (*11*), it must be facing the external aqueous medium. Given its localization within the same putative external loop as 163, 166, and 173 and the fact that these three residues behave as if they are able to repel Na^+ (*9*), a plausible synthesis of the experimental results is that position 170 lies within a Na^+ interaction "pore" or cleft, but it is located distally or deeper than neighboring residues 163, 166, and 173, which are located closer to the entrance of the Na^+ binding site. Thus, negative charge at position 170, such as the glutamate residue, could enhance binding of Na^+ which has entered the pore. Further, since position 170 is very sensitive to the nature and size of the moiety bearing the negative charge, it must be situated in a region of the transporter that measures the electric field and, therefore, is sensitive to membrane potential.

It is also worth drawing attention to a convergence of several observations for Q170E time constants. (i) τ_{fast}, which was previously shown in wt SGLT1 to reflect the fast, charge-dependent, transition of empty carrier, is not observed for Q170E; (ii) the transporter prefers an outside-facing conformation, which is exaggerated at 100 mM Na^+ compared to 10 mM Na^+; (iii) τ_{slow} is reduced (i.e., is faster) and shows voltage independence at negative potentials in the presence of 100 mM Na^+ (which promotes an outside-facing conformation), but voltage dependence is restored at hyperpolarization with 10 mM Na^+ (which promotes an inside-facing conformation). Collectively, these findings can be explained if it is postulated that the mutation affects the fast transition component of the empty carrier, and what we are observing with Q170E τ_{slow} (i.e., becoming faster) is the residual empty carrier slow transition with the fast, charge-dependent transition removed (within the context of our clamp speed).

The results of the computer simulations provide further support for our interpretation that the glutamine to glutamate mutation results in increased Na^+ affinity. As described in the Results section and presented in Table 1, the most marked change in the computer simulation derived parameters can be traced to an increase in the binding rate for Na^+ (k_{21} in Figure 10). This correlates well with the measured Q170E K_{Na} and its voltage dependency compared to Q170C and wt.

A possible explanation for the disparity between the 10 mM $Q(V_t)$ curve and the simulated Boltzmann relation in Figure 4B might be an underestimation by the model of the z_{34} value. Simulation predicts that the Q170E z_{34} value goes to zero (Table 1), compared to 0.31 for wt rSGLT1 (*13*). Despite this discrepancy, overall there appears to be reasonable agreement between experimental and computer simulations based on a four-state model, depicted in Figure 10.

Further insights require continuing structure/function studies in this interesting domain of rSGLT1.

REFERENCES

1. Hediger, M. A., Coady, M. J., Ikeda, T. S., and Wright, E. M. (1987) Expression cloning and cDNA sequencing of the Na^+/glucose cotransporter, *Nature 330*, 379−381.
2. Chen, X. K., Coady, M. J., and Lapointe, J. Y. (1996) Fast voltage clamp discloses a new component of presteady-state currents from the Na^+-glucose cotransporter, *Biophys. J. 71*, 2544−2552.
3. Parent, L., Supplisson, S., Loo, D. D., and Wright, E. M. (1992) Electrogenic properties of the cloned Na^+/glucose cotransporter: I. Voltage-clamp studies, *J. Membr. Biol. 125*, 49−62.
4. Loo, D. D., Hazama, A., Supplisson, S., Turk, E., and Wright, E. M. (1993) Relaxation kinetics of the Na^+/glucose cotransporter, *Proc. Natl. Acad. Sci. U.S.A. 90*, 5767−5771.
5. Zampighi, G. A., Kreman, M., Boorer, K. J., Loo, D. D., Bezanilla, F., Chandy, G., Hall, J. E., and Wright, E. M. (1995) A method for determining the unitary functional capacity of cloned channels and transporters expressed in *Xenopus laevis* oocytes, *J. Membr. Biol. 148*, 65−78.
6. Panayotova-Heiermann, M., Loo, D. D., Lostao, M. P., and Wright, E. M. (1994) Sodium/D-glucose cotransporter charge movements involve polar residues, *J. Biol. Chem. 269*, 21016−21020.
7. Panayotova-Heiermann, M., Eskandari, S., Turk, E., Zampighi, G. A., and Wright, E. M. (1997) Five transmembrane helices form the sugar pathway through the Na^+/glucose cotransporter, *J. Biol. Chem. 272*, 20324−20327.
8. Panayotova-Heiermann, M., Loo, D. D., Kong, C. T., Lever, J. E., and Wright, E. M. (1996) Sugar binding to Na^+/glucose cotransporters is determined by the carboxyl-terminal half of the protein, *J. Biol. Chem. 271*, 10029−10034.
9. Lo, B., and Silverman, M. (1998) Cysteine scanning mutagenesis of the segment between putative transmembrane helices IV and V of the high affinity Na^+/glucose cotransporter SGLT1, *J. Biol. Chem. 273*, 29341−29351.
10. Lo, B., and Silverman, M. (1998) Replacement of Ala-166 with cysteine in the high affinity rabbit sodium/glucose transporter alters transport kinetics and allows methanethiosulfonate ethylamine to inhibit transporter function, *J. Biol. Chem. 273*, 903−909.
11. Huntley, S. A., Krofchick, D., and Silverman, M. (2004) Position 170 of rabbit Na^+/glucose cotransporter (rSGLT1) lies in the Na^+ pathway; modulation of polarity/charge at this site regulates charge transfer and carrier turnover, *Biophys. J. 87*, 295−310.
12. Krofchick, D., Huntley, S. A., and Silverman, M. (2004) Transition states of the high-affinity rabbit Na^+/glucose cotransporter SGLT1 as determined from measurement and analysis of voltage-dependent charge movements, *Am. J. Physiol. Cell Physiol. 287*, C46−C54.
13. Krofchick, D., and Silverman, M. (2003) Investigating the conformational states of the rabbit Na^+/glucose cotransporter, *Biophys. J. 84*, 3690−3702.
14. Glasstone, S., Laider, K. J., and Eyring, H. (1941) *The Theory of Rate Processes*, 1st ed., McGraw-Hill, New York.

BI052267M